
# Ultralow-noise preamplified optical receiver using conventional single-wavelength transmission

Research Article Vol. 11, No. 11 / November 2024 / Optica 1497


# Ultralow-noise preamplified optical receiver using conventional single-wavelength transmission

Rasmus Larsson,[1,*] Ruwan U. Weerasuriya,[1,2] and Peter A. Andrekson[1]

[1]Department of Microtechnology and Nanoscience, Chalmers University of Technology, Kemivägen 9, Gothenburg, Sweden
[2]Department of Electronic and Telecommunication Engineering, University of Moratuwa, Moratuwa, Sri Lanka
*rasmus.larsson@chalmers.se

Received 14 August 2024; revised 2 October 2024; accepted 3 October 2024; published 28 October 2024

**Conventional optical amplifiers that use stimulated emission suffer from the generation of excess noise, thus limiting the performance in many applications. The phase-sensitive optical parametric amplifier, relying on the use of a nonlinear material for amplification, is an exception that can approach a noise figure of 0 dB. Its implementation in optical communication links has, however, been cumbersome due to increased complexity both in the transmitter and the receiver, effectively limiting the use of such amplifiers in practice. Here, we propose and demonstrate an implementation of a transmission system with exceptional performance in terms of receiver sensitivity (0.9 photons per bit) using a standalone ultralow-noise phase-sensitively preamplified receiver and a conventional single-wave optical transmitter. This is a significant simplification compared to previous demonstrations and can transform such amplifiers from a curiosity to practical use for example in deep-space-to-earth communication links.**



https://doi.org/10.1364/OPTICA.539544

## 1. INTRODUCTION

For coherent reception of weak optical signals, sensitive receivers typically use optical pre-amplification as it boosts the signal to noise ratio (SNR) close to the shot-noise limit. Although an ideal homodyne coherent receiver enables shot-noise limited detection in principle (without optical amplification), the limited quantum efficiency in practical photo-detectors as well as the 3 dB SNR loss in dual-quadrature coherent receivers (compared to single-quadrature detection) [1] prohibits this in practice. Optical amplifiers, such as the erbium doped fiber amplifier (EDFA), help overcome these limitations and therefore find wide use in photonics applications. They enable ease of use and simple implementation into measurement and communications systems.

Stimulated-emission-based amplifiers like the EDFA have a quantum limited noise figure (NF) of 3 dB in theory and can at best provide 3 dB worse SNR than the ideal shot-noise limited single-quadrature homodyne coherent receiver when used as preamplifiers. Optical parametric amplifiers (OPAs) have a unique advantage over such conventional amplifiers in that they can amplify a signal with a NF well below (better than) this 3 dB quantum limit [2] (lowest measured NF = 1 dB [3,4]), when operated in phase-sensitive mode. Great interest in the "noiseless" amplification of phase-sensitive parametric amplifiers (PSAs) has developed in areas of optical free-space communications [5], fiber-optical transmission links [6], signal processing [7,8], and quantum metrology [9]. However, despite the great appeal for noiseless amplification and a theoretical 0 dB NF-limit (ideal shot-noise limited receiver performance), the photonics community still lacks a simple and practical adaptation of low-noise PSAs into a single input-output amplifier module, like the EDFA, that is compatible with conventional systems.

In demonstrated PSAs to date, optical amplification has been facilitated either via nonlinear three- [10] or four-wave mixing (FWM) [11] that incorporates one or several high-power pump waves in addition to weak signal and idler waves. The relative phase between waves determines the direction of power transfer, hence, a power transfer from pump to signal, and a <3 dB NF is only achieved for phase-locked waves. This requirement becomes a significant challenge for realistic systems, like a communication link, where signal and idler(s) are generated at the transmitter while the pump wave is created at the receiver, using independent and uncorrelated lasers.

In previous demonstrations, phase-locked pumps have been generated with carrier recovery of either a transmitter-generated pump reference (co-propagated alongside the signal) or a tapped part of the received signal, together with optical injection locking (OIL) [12] or optical phase-locked loops (OPLLs) [13–15]. Tapping part of the received signal directly degrades the "black-box" NF of the PSA, as does the power allocated in a pump-reference wave. The creation of a pump-reference wave also complicates the transmitter implementation.

Recently, we demonstrated in [16] a lossless receiver-side local pump-generation scheme that achieves phase-locking via gain-maximization of the PSA, avoiding the excess losses associated with previous solutions. The PSA utilized FWM in a highly nonlinear fiber (HNLF) with a degenerate-pump signal and

idler-wave configuration. While this type of PSA has previously demonstrated a low 1.1 dB NF [4] as well as a record one photon per information-bit (PPIB) receiver sensitivity [5], it requires the transmitter to generate both the signal and its conjugated idler copy. This brings added hardware complexity compared to a typical single-wavelength transmitter and limits the use of such PSAs in conventional systems as a "black-box" preamplifier. This is especially in the interest for space-laser-communication downlinks to earth, where low-complexity spacecraft transmitters are necessary and where PSA-enabled, high-sensitivity receivers could boost the data rate compared to current photon-counting receiver technologies [17,18].

Black-box operated PSA amplification of a single transmitted wave has been demonstrated in [14,15] (based on three-wave mixing); however, in addition to being limited by signal-tapping prior to amplification, OPLL operation was only demonstrated at received powers $> -40$ dBm, which significantly limits the use and potential of the PSA as a preamplifier for weak signals.

In this work, we demonstrate a single-wave solution in the form of a dual-pump, degenerate-signal PSA using lossless locking (as in [16]) at down to −67 dBm received powers, with a "black-box" NF of 1.7 dB and a predicted post-forward error correction (FEC) receiver sensitivity well below (better than) 1 PPIB. This is the lowest reported pre-FEC sensitivity to date for coherent reception. This is also the first time a FWM-based single-wave PSA is demonstrated with a <3 dB NF. The PSA-process, shown in Fig. 1(a), utilizes two strong pumps to amplify a central degenerate signal. The single-wave operation makes the dual-pump PSA a truly self-contained "black-box" optical preamplifier compatible with conventional optical communication systems, like the one shown in Fig. 1(b). Here the transmitter consists of a laser and an external modulator that sends the signal through a lossy channel before amplification in the PSA and subsequent coherent detection.

The degenerate-signal aspect of the PSA makes it a single-quadrature amplifier, compatible with binary-phase-shift keying (BPSK) modulation formats. However, with no added hardware complexity, we show how the PSA can operate with arbitrary modulation formats by also demonstrating the phase-sensitive amplification of a quadrature-phase-shift keyed (QPSK) signal with the use of dual-carrier modulation, as has been shown for a three-wave mixing PSA in [15].

In low-SNR communications, where low-noise amplification is desirable, the capacity-gain from higher-order modulation is similar to that of wavelength division multiplexing (see Supplement 1, Section 7). Hence, the restriction to low-noise amplification of a single wavelength will not be substantially limiting for such applications.

An important challenge in achieving the low NF is the reduction of additional and undesired FWM-processes of two pumps that transfers excess vacuum noise onto the signal. Next, we address this further before presenting the experimental implementation, the results, and a concluding discussion in the following sections.

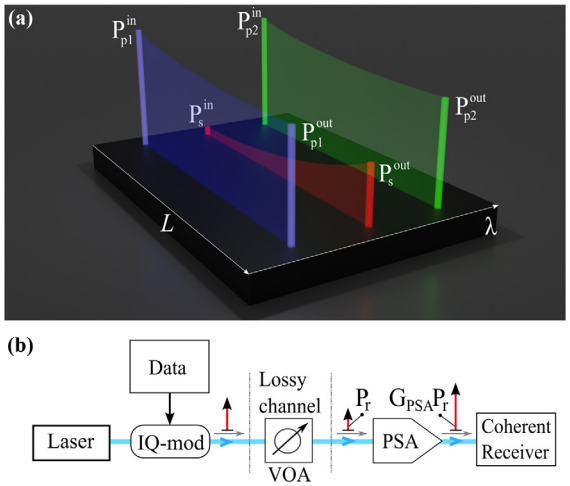


**Fig. 1.** (a) Evolution of FWM-based amplification for a dual-pump, degenerate-signal PSA. λ, wavelength; $L$, propagation length. (b) A schematic of a typical optical communication system with a PSA as a "black-box" preamplifier. IQ-mod, in-phase and quadrature-phase electro-optic modulator; VOA, variable optical attenuator. $P_r$, received power; $G_{PSA}$, phase sensitive gain.

## 2. SUPPRESSION OF UNDESIRED FWM-PROCESSES

To reach a low NF for the dual-pump, degenerate-signal PSA the FWM-processes that incorporate both signal and higher-order idlers i1 and i2 (see Fig. 2) must be suppressed. This is to minimize excess vacuum-noise transfer from i1 and i2 to the signal, while simultaneously promoting the desired FWM-process. To achieve this, both signal and pump wavelengths must be chosen carefully based on the FWM phase-matching conditions, given the dispersion profile of the HNLF, its nonlinear constant, as well as the pump power used. This wavelength selection process has been studied theoretically and numerically in [19–21] where it is indicated that the optimal wavelength configuration is found for a center (signal) wavelength $\lambda_c$ at, or slightly on the short-λ side of, the zero-dispersion wavelength of the HNLF while also selecting a wide pump wavelength separation of several tens of nanometers.

This finding proved useful as an optimal center (signal) wavelength at $\lambda_c = 1561.45$ nm and pump separation of 50.5 nm was found by sweeping the center wavelength close to the 1561.7 nm zero-dispersion wavelength of the HNLF. Further details on the sweep, pump power, and HNLF parameters are found in Supplement 1.

## 3. EXPERIMENAL IMPLEMENTATION

The setup was designed to demonstrate the "black-box" operation of the PSA and for investigating its performance. It used the setup in Fig. 1(b) as the optical link, where a $2^{15}-1$ bit long pseudo random bit sequence pattern from an arbitrary waveform generator (AWG) was used to modulate the signal at a symbol rate of 10 Gbaud BPSK [Fig. 3(a)] or dual-carrier QPSK [Fig. 3(b)] in the external IQ-modulator. In the case of the dual-carrier signal, the QPSK signal and its conjugated copy (idler) were shifted $\Delta f = 6$ GHz and −6 GHz, respectively. Note that for both BPSK and dual-carrier QPSK, only one quadrature is used for modulation; hence in practice a simple Mach–Zehnder modulator would suffice. To alter the received signal power $P_r$ a variable optical

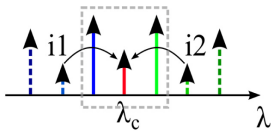


**Fig. 2.** Illustration of several simultaneous FWM tones for a dual-pump, degenerate-signal PSA.

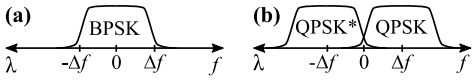


**Fig. 3.** (a) Illustration of the optical signal spectrum for the BPSK signal and (b) the dual-carrier QPSK signal. $\Delta f = 6$ GHz.

attenuator (VOA) was used and represented a lossy transmission channel.

The "black-box" PSA itself is depicted in Fig. 4(a). To obtain high PSA gain the HNLF needs to be pumped with high optical power, which makes the amplification process susceptible to stimulated Brillouin scattering (SBS) [22]. SBS limits the achievable gain, and hence, the effective NF of the PSA. To suppress SBS, the two pumps are counter-phase modulated [23] using three sinusoidal tones as described in Supplement 1, Section 2.

The modulated pumps are amplified in high-power C- and L-band EDFAs before being optically filtered and combined through a wavelength division multiplexer (WDM) into a total pump power of 30.1 dBm (27.1 dBm per pump). The pumps and the received signal $P_r$ are then combined in a WDM before phase-sensitive amplification ensues in the 350 m long HNLF. A 1% tap provided the HNLF output for optical spectrum analysis using an optical spectrum analyser (OSA). On the 99%-port the amplified signal was filtered out before a 10% tap provided a photo-detector (PD) and the OPLL with the optical error signal. This kept the PSA phase-locked, using phase control and frequency control of $\phi$-mod and pump 2, respectively, via the local pump-generation scheme [16].

In our demonstration, the use of $\phi$-mod helped reduce the phase control loop delay (see Supplement 1); however, $\phi$-mod would not be needed in a dedicated system (with appropriate lasers; see Supplement 1) and phase and frequency control can instead

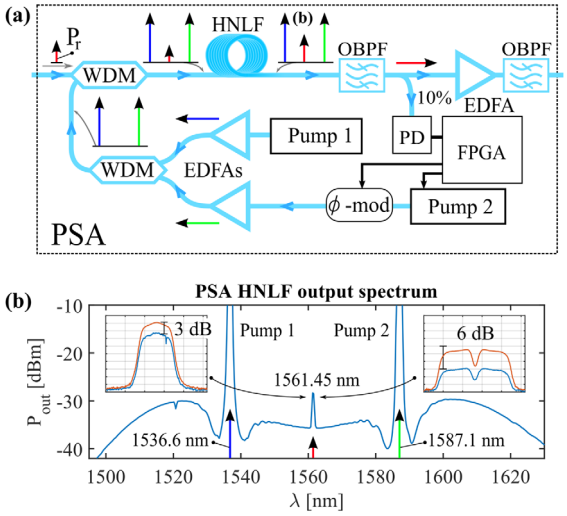


**Fig. 4.** (a) Schematic of the "black-box" PSA. Polarization controllers were used to align the polarization of all waves at all points. WDM, wavelength division multiplexer; OBPF, optical band-pass filter; PD, photo-detector; FPGA, field-programmable gate array. $\phi$-mod, electro-optic phase modulator. Direct frequency control of pump 2 and phase control in $\phi$-mod enabled PSA phase-locking. (b) Measured PSA-HNLF optical output spectrum with 0.5 nm resolution. Insets show the unlocked (blue) versus phase-locked (orange) amplified BPSK signal to the left and to the right the PIA (blue) versus PSA case (orange) of the amplified dual-carrier QPSK signal, both with 0.01 nm resolution. In this PIA case for QPSK, only the signal and no idler [QPSK* in Fig. 3(b)] is present at the HNLF input, i.e., single-sideband input and with $P_r$(PIA) = $P_r$(PSA)/2.

be implemented using direct proportional and integral current control of pump laser 2, respectively. This would circumvent the practical limitations of $2\pi$-phase jumps in $\phi$-mod (during which phase is out of lock) due to voltage range saturation.

Of note is our use of low-noise lasers (~100 Hz linewidth) for generating signal and pumps in our demonstration to achieve phase-locking down to −67 dBm received powers. The need for low-noise lasers at low received powers stems from the fundamental bandwidth-SNR trade-off for any locking system. While the local pump-generation scheme offers non-invasive (lossless) phase-locking and significantly reduces the implementation complexity, compared to previous solutions, its OPLL bandwidth is also limited by the inclusion of the PSA length into the control loop. The restricted OPLL bandwidth due to the added (in our case 350 m) loop delay poses another limitation to the use of low-noise lasers also at high received powers (unless the PSA can be miniaturized).

To evaluate the performance of the phase-locking, both a reference PSA case (PSA REF), with correlated pump and signal waves, in addition to the local pump locking case (PSA LP), with phase-locking of independent pump and signal waves, were investigated. This was done for both the BPSK and QPSK signals. For comparison, a QPSK case with only one of the carriers active was also investigated [i.e., with QPSK* removed in Fig. 3(b)]. This case is referred to as a phase-insensitive amplifier (PIA) and has an ideal NF of 3 dB.

From the OSA measured HNLF output spectra [see example in Fig. 4(b)] the gain of the parametric amplification in the HNLF was estimated as $G_{\mathrm{PIA}} = 19 \pm 1$ dB and $G_{\mathrm{PSA}} = 22 \pm 1$ dB for the PIA and PSA cases, respectively (see Supplement 1, Section 3). The uncertainty in gain was estimated to be ±1 dB due to the slight drift of the PSA pump power and the resulting gain variation. Note that this gain is defined with respect to the total input power (including idler if present). The NF of this amplification was also estimated using the OSA measured spectra and is covered in Supplement 1, Section 3. The "black-box" NF, important to a practical implementation, was instead extracted from the bit error rate (BER)-measurements discussed shortly.

The insets in Fig. 4(b) demonstrate the phase-sensitive gain of the PSA. The left inset compares the measured HNLF output average signal power between the phase-locked and free-running BPSK PSA, showing the expected 3 dB improvement from phase-locking. Meanwhile, the right inset compares the QPSK PIA and phase-locked QPSK PSA with respect to the ideal 6 dB improvement [4] (+3 dB from idler and +3 dB from phase-locking).

For BER-measurements the preamplified signal was optically filtered and combined with a local oscillator (LO) of 1 MHz linewidth in an intradyne dual-quadrature coherent receiver. Observe that with optical pre-amplification, detection is limited by the amplified optical vacuum noise, which suffers the same losses and detection inefficiencies in a dual-quadrature receiver as the signal, thus rendering the effect of such practical limitations insignificant to the SNR. For effective digital filtering of the noise, care was taken to match the LO wavelength as close as possible to the signal wavelength. In the dual-carrier case only the signal carrier is detected; hence, the LO was shifted $\Delta f = 6$ GHz (see Fig. 3) to recover the QPSK signal. For each received power a number of batches of size 500,000 symbols were captured in a real-time scope and processed offline using digital signal processing (DSP) [24] based on QAMpy [25], which involved: resampling, IQ-imbalance

and frequency offset compensation, constant modulus, and carrier phase estimation as described in [24]. In the case of BPSK, the constant modulus equalizer filter taps were calculated for a generated digital copy of the received signal, consisting of the sampled signal plus a delayed and 90 deg rotated copy of the signal (to mimic QPSK).

## 4. RESULTS

In Fig. 5 we present the measured BER versus received signal power $P_r$, both in dBm and photons per bit (PPB), using the "black-box" PSA as a preamplifier, for the BPSK cases. Included for comparison is also an EDFA-preamplified receiver with $NF_{EDFA} = 4.2 \pm 0.1$ dB as well as theoretical curves of different NFs. Note that the 0 dB NF represents the ideal PSA-preamplified receiver, which has equivalent performance to that of an ideal shot-noise limited single-quadrature homodyne coherent receiver. The experimental curves are averaged from the $M$ out of $N$ number of batches with the lowest BER, with $M/N = 5/10$, 10/20, and 10/30 for the EDFA, PSA REF, and PSA LP cases, respectively. The occasional divergence of the DSP as well as the occurrence of $2\pi$-phase jumps in $\phi$-mod of Fig. 4(a) directly impact some of the measured batches; hence using an $M/N$ ratio for statistical averaging is more representative of the actual BER performance (see Supplement 1, Section 3) as these effects can be circumvented with optimized DSP and direct laser-phase control in a practical system. The "black-box" NF was estimated by fitting theoretical curves of given NF to the measured BER-curves at low received powers.

In Fig. 5 the PSA REF and PSA LP BPSK performance matches that of theoretical 1.25 dB and 1.5 dB NF-curves, respectively, where no other penalties are assumed. The 0.25 dB NF-difference between REF and LP cases represents the NF-penalty due to imperfect locking in the LP case. Moreover, we demonstrate a close to 3 dB NF-reduction between the EDFA and PSA cases, demonstrating the improvement in NF beyond the conventional 3 dB limit.

In the bottom-left inset of Fig. 5 a 14% BER is emphasized. This is the pre-FEC BER-limit below which one can reach error-free transmission (BER$< 10^{-6}$) at 100% FEC overhead, as shown in [5,26]. From this, the error-free receiver sensitivity, assuming 100% FEC overhead, is estimated as 0.79 ($-1.05 \pm 0.1$ dB) and 0.83 ($-0.8 \pm 0.1$ dB) PPIB for the BPSK PSA REF and PSA LP, respectively, as 1PPIB = 2PPB (+3 dB) with 100% FEC overhead. For the 10 Gb/s transmitted BPSK this corresponds to approximately $-63$ dBm received power.

Like for the BPSK case, the QPSK BER is similarly presented in Fig. 6, including the PIA case. Here, the PSA REF, PSA LP, and PIA performance matches that of theoretical 1.7 dB, 1.9 dB, and 4.3 dB NF-curves, respectively, in the low received power-limit. As for the BPSK case, a close to 3 dB NF reduction between PIA, EDFA, and PSA cases is shown. We also see, however, an added ∼0.4 dB NF penalty compared to the BPSK case. The increasing NF penalty for larger $P_r$ is partly due to the limited pump OSNR in our system, which degrades BER in proportion to signal power [27,28]. The ∼0.4 dB penalty increase from BPSK to QPSK is likely partially due to the larger optical signal bandwidth (which suffers more from chromatic dispersion, optical filter shaping, etc.) together with the added sensitivity to phase noise for QPSK modulation. Despite the extra penalty, it is clear that the PSA preamplified receiver can be used for non-binary modulation formats such as QPSK while retaining well below (better than) conventional quantum limited (<3 dB) NF.

Similar to before, from the left-most inset in Fig. 6, the error-free receiver sensitivity at 100% FEC overhead, is predicted as 0.87 ($-0.6 \pm 0.1$ dB) and 0.91 ($-0.4 \pm 0.1$ dB) PPIB for the QPSK PSA REF and PSA LP, respectively.

Uncertainty in NF and sensitivity measurements is estimated to be 0.1 dB and is limited by the 0.1 dB uncertainty of the power meters used to calibrate the PSA input and output to their respective power monitor ports.

Finally, in Table 1 we present a summary of the estimated NF (and sensitivity) penalty due to imperfect phase-locking, dual-carrier modulation, as well as additional penalties (see Supplement 1) induced by limited HNLF gain, pump phase modulation for SBS-suppression, and non-zero WDM insertion loss (which so far has not been included).

The final PSA "black-box" NF, including the WDM loss and phase-locking penalty, is $1.7 \pm 0.1$ dB for the BPSK signal and $2.1 \pm 0.1$ dB for the QPSK signal. The 2.1 dB NF for QPSK (with

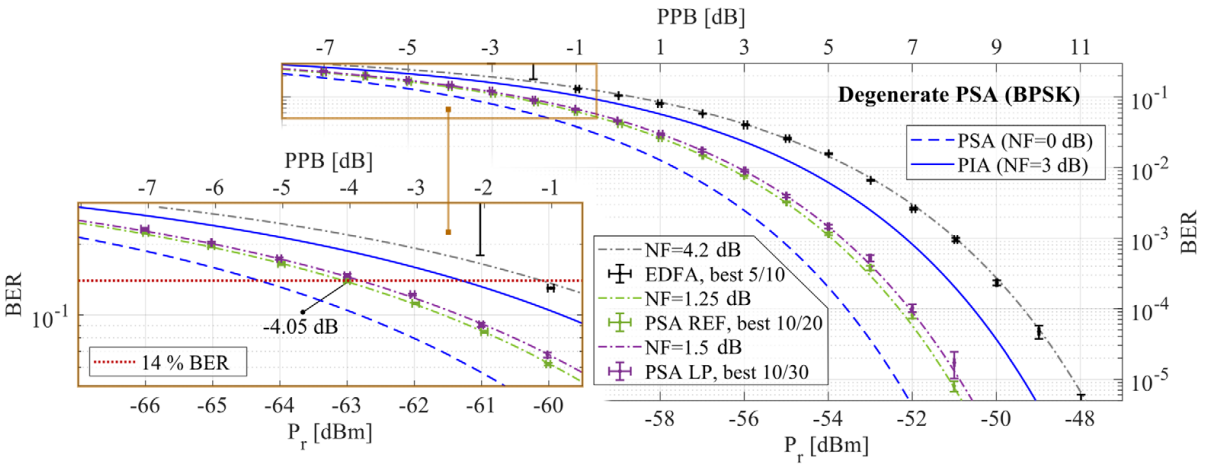


**Fig. 5.** BER versus received power (both in dBm and PPB) for the BPSK signal with standard deviation error bars. The mean BER was calculated from a portion of the total number of captured batches with the lowest BER-values, as shown in the figure legend. Theoretical BER curves for different NFs are included for comparison. PSA LP: the realistic case with local-pump locking for uncorrelated signal and pumps. PSA REF: a reference case with correlated signal and pumps (avoiding locking penalties).

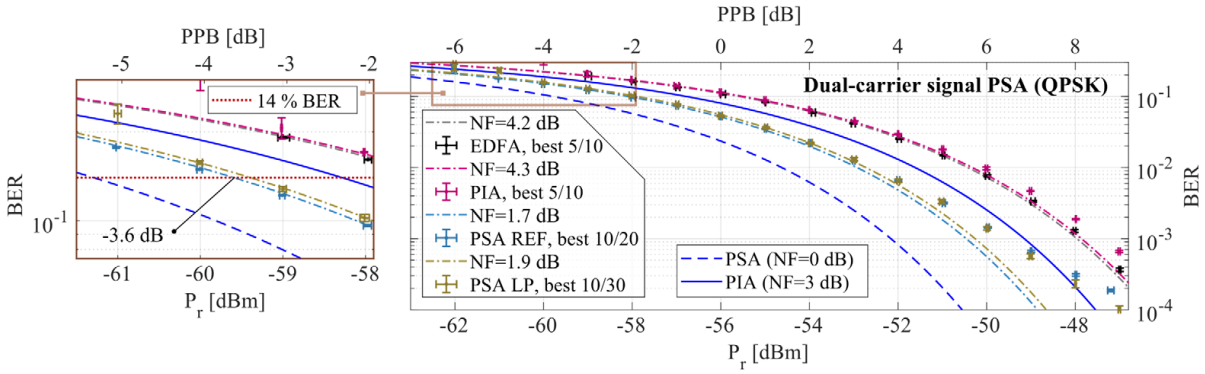


**Fig. 6.** BER versus received power (both in dBm and PPB) for the QPSK signal with standard deviation error bars. The mean BER was calculated from a portion of the total number of captured batches with the lowest BER-values, as shown in the figure legend. Theoretical BER curves for different NFs are included for comparison. PSA LP: the realistic case with local-pump locking for uncorrelated signal and pumps. PSA REF: a reference case with correlated signal and pumps (avoiding locking penalties).

**Table 1. Estimated NF and Sensitivity Penalties[a]**

| Penalty | Δ NF [dB] | Affected Cases |
|---|---|---|
| Limited gain | 0.05 | All |
| Phase-locking | 0.25 | PSA LP |
| Pump modulation | 0.2 | PSA REF, PSA LP |
| WDM loss | 0.2 | All |
| Dual-carrier | 0.4 | QPSK |

[a]The "affected cases" column specifies which cases were affected by the corresponding penalty. Uncertainty of stated values is ±0.05 dB.

all penalties included) is similar to the NF reported in [5] (1.2 dB, measured using an OSA) when including the stated penalties of 0.4 dB (transmitter and receiver implementation penalty), 0.2 dB (WDM loss), and 0.3 dB (pump-reference power and phase-locking penalty).

Next, the estimated final "black-box" receiver sensitivities are 0.87 ($-0.6 \pm 0.1$ dB) and 0.96 ($-0.2 \pm 0.1$ dB) PPIB for the BPSK and QPSK signal, respectively (again based on the result in [5]). This is 2.4 dB and 2.8 dB worse than the theoretical best sensitivity (at the spectral efficiency used) of 0.5 PPIB for the BPSK and QPSK signal, respectively (see Supplement 1, Section 8). These sensitivities are comparable to (QPSK), or better than (BPSK), the previous 1 PPIB receiver sensitivity record in [5] (using 10.52 Gbaud QPSK) for coherent detection, thus demonstrating a new record pre-FEC BER performance and a better than 1 PPIB receiver sensitivity potential.

## 5. DISCUSSION AND CONCLUSION

We have, for the first time, experimentally demonstrated a below 3 dB NF-PSA for single-wave amplification based on FWM. Both BPSK and QPSK data signals were used, showing the degenerate PSA's compatibility with arbitrary modulation formats, like in [15]. The feature of single-wave amplification enables the PSA as a self-contained "black-box" preamplifier, ready for use in conventional single-wavelength optical communication systems.

The demonstrated PSA BER performance predicts a post-FEC receiver sensitivity of 0.9 PPIB, which is better than the current record demonstration in [5]. Although a much lower 0.08 PPIB sensitivity has been demonstrated using photon-counting detection in [29], the detection bandwidth, and hence achievable data rate (in this case 14 kb/s), is very limited in such receivers [18,30]. Thus, for space-laser-communication downlinks to earth, where high-speed, single-wave transmission is desirable and where photon-counting has mainly been considered [17], the demonstrated "black-box" PSA could significantly improve the data rate (>10 Gb/s) while retaining an excellent sensitivity.

While the experiment revolved around 10 Gbaud BPSK and QPSK transmission, with error-free detection at received powers above −63 dBm and −60 dBm, respectively, lower received powers can be detected error-free at lower bit-rates at the same sensitivities. However, the OPLL SNR is not only limited by the signal bandwidth but also the laser phase noise bandwidth, i.e., its performance will degrade/improve with lower/higher received powers despite maintaining the number of photons per bit. Therefore, the OPLL operation at low received powers strongly benefits from the use of low-linewidth lasers. This limitation, however, goes hand in hand with that of the DSP phase-recovery at low powers and should be considered as a general requirement for reaching the lowest possible receiver sensitivity.

Another limitation of the demonstrated PSA stems from the necessary confinement of the signal wavelength close to the HNLF zero-dispersion wavelength to achieve low NF. This limits the low-noise PSA bandwidth for a given HNLF. While other HNLFs can be used to accommodate other wavelengths, the implementation of FWM-type PSAs on a silicon nitride (SiN) chip-based platform [31] may provide the freedom in dispersion engineering to enable a much wider low-noise bandwidth for the dual-pump, degenerate-signal PSA. The same chip-based platform will also avoid SBS and the pump-phase-modulation penalty, as well as reduce the effective PSA length and help eliminate the added phase-locking penalty imposed by the 350 m HNLF that dominates the OPLL loop delay.

Further steps towards a practical system, which would also improve the performance of the PSA, pertain to the minimization of the counter-phase modulation mismatch between pumps and the use of low-noise lasers at the appropriate pump wavelengths, the latter, to avoid added OPLL loop delay from wavelength-conversion stages used here, as well as phase jumps in the phase control. With the use of lower-insertion-loss WDMs (<0.1 dB signal coupling loss) and minimized HNLF splice loss the "black-box" NF can be improved further. All in all, with mentioned steps taken, a final "black-box" PSA NF of 1.0 dB (or 0.74 PPIB sensitivity) may be realistically attainable in a HNLF (lower in SiN), which

in the form of a self-contained, single-wave preamplifier may open up new possibilities for sensitive reception in optical free-space communications [5], sensing [32], and quantum metrology [9].

**Funding.** Vetenskapsrådet (VR-2015-00535).

**Acknowledgment.** We thank Z. He for help with implementing the dual-carrier modulation and assistance in the lab, C. Skehan for assistance in building the pump wave-generation setup, M. Karlsson for discussions on the dual-pump, degenerate-signal PSA and J. Schröder for discussions on the digital signal processing for BPSK.

**Disclosures.** The authors declare that there are no conflicts of interest related to this article.

**Data availability.** Data underlying the results presented in this paper are available in Ref. [33].

**Supplemental document.** See Supplement 1 for supporting content.

## REFERENCES

1. K. Banaszek, L. Kunz, M. Jachura, *et al.*, "Quantum limits in optical communications," J. Lightwave Technol. **38**, 2741–2754 (2020).
2. C. M. Caves, "Quantum limits on noise in linear amplifiers," Phys. Rev. D **26**, 1817–1839 (1982).
3. T. Kazama, T. Umeki, S. Shimizu, *et al.*, "Over-30-dB gain and 1-dB noise figure phase-sensitive amplification using a pump-combiner-integrated fiber i/o ppln module," Opt. Express **29**, 28824–28834 (2021).
4. Z. Tong, C. Lundström, P. A. Andrekson, *et al.*, "Towards ultrasensitive optical links enabled by low-noise phase-sensitive amplifiers," Nat. Photonics **5**, 430–436 (2011).
5. R. Kakarla, J. Schröder, and P. A. Andrekson, "One photon-per-bit receiver using near-noiseless phase-sensitive amplification," Light Sci. Appl. **9**, 153 (2020).
6. S. L. Olsson, H. Eliasson, E. Astra, *et al.*, "Long-haul optical transmission link using low-noise phase-sensitive amplifiers," Nat. Commun. **9**, 2513 (2018).
7. R. Slavík, F. Parmigiani, J. Kakande, *et al.*, "All-optical phase and amplitude regenerator for next-generation telecommunications systems," Nat. Photonics **4**, 690–695 (2010).
8. M. A. Foster, R. Salem, D. F. Geraghty, *et al.*, "Silicon-chip-based ultrafast optical oscilloscope," Nature **456**, 81–84 (2008).
9. F. Hudelist, J. Kong, C. Liu, *et al.*, "Quantum metrology with parametric amplifier-based photon correlation interferometers," Nat. Commun. **5**, 3049 (2014).
10. K. J. Lee, F. Parmigiani, S. Liu, *et al.*, "Phase sensitive amplification based on quadratic cascading in a periodically poled lithium niobate waveguide," Opt. Express **17**, 20393–20400 (2009).
11. Z. Tong, C. Lundström, P. A. Andrekson, *et al.*, "Ultralow noise, broadband phase-sensitive optical amplifiers, and their applications," IEEE J. Sel. Top. Quantum Electron. **18**, 1016–1032 (2012).
12. R. Kakarla, J. Schröder, and P. A. Andrekson, "Optical injection locking at sub nano-watt powers," Opt. Lett. **43**, 5769–5772 (2018).
13. R. Larsson, K. Vijayan, and P. A. Andrekson, "Zero-offset frequency locking of lasers at ultra-low optical powers," in *Optical Fiber Communications Conference and Exhibition (OFC)* (2023), pp. 1–3.
14. S. Shimizu, T. Kobayashi, T. Kazama, *et al.*, "Optical phase-sensitive amplification of higher-order qam signal with single Mach–Zehnder amplitude modulator," Electron. Lett. **57**, 32–33 (2021).
15. S. Shimizu, T. Kazama, T. Kobayashi, *et al.*, "Non-degenerate phase-sensitive amplification scheme using digital dispersion pre-equalization for unrepeated transmission," Opt. Express **29**, 8451–8461 (2021).
16. R. Larsson, K. Vijayan, J. Schröder, *et al.*, "Low-noise phase-sensitive optical parametric amplifier with lossless local pump generation using a digital dither optical phase-locked loop," Opt. Express **31**, 36603–36614 (2023).
17. M. E. Grein, A. J. Kerman, E. A. Dauler, *et al.*, "An optical receiver for the Lunar Laser Communication Demonstration based on photon-counting superconducting nanowires," Proc. SPIE **9492**, 949208 (2015).
18. H. Hao, Q.-Y. Zhao, Y.-H. Huang, *et al.*, "A compact multi-pixel superconducting nanowire single-photon detector array supporting gigabit space-to-ground communications," Light Sci. Appl. **13**, 25 (2024).
19. Y. Bouasria, D. Chatterjee, W. Xie, *et al.*, "Investigation of the noise figure in a degenerate dual-pump phase-sensitive amplifier using a multi-wave model," J. Opt. Soc. Am. B **37**, 2745–2754 (2020).
20. K. Inoue, "Phase matching condition of dual-pump phase-sensitive amplification in optical fiber," in *Opto-Electronics and Communications Conference (OECC) and Photonics Global Conference (PGC)* (2017), pp. 1–2.
21. K. Inoue, "Influence of multiple four-wave-mixing processes on quantum noise of dual-pump phase-sensitive amplification in a fiber," J. Opt. Soc. Am. B **36**, 1436–1446 (2019).
22. M. E. Marhic, *Prospects for Future Developments* (Cambridge University, 2007), pp. 315–332.
23. A. Bolle, G. Grosso, A. Cosentino, *et al.*, "Influence of phase modulation on the brillouin gain curve," in *14th European Conference on Optical Communication, ECOC 88 (Conf. Publ. No.292)* (1988), Vol. **1**, pp. 119–122.
24. S. J. Savory, "Digital filters for coherent optical receivers," Opt. Express **16**, 804–817 (2008).
25. J. Schröder, M. Mazur, and M. Brehler, "Chalmersphotonicslab/qampy: v0.2," (2019).
26. A. Alvarado, E. Agrell, D. Lavery, *et al.*, "Replacing the soft-decision FEC limit paradigm in the design of optical communication systems," J. Lightwave Technol. **33**, 4338–4352 (2015).
27. P. Kylemark, P. O. Hedekvist, H. Sunnerud, *et al.*, "Noise characteristics of fiber optical parametric amplifiers," J. Lightwave Technol. **22**, 409–416 (2004).
28. A. Durecu-Legrand, C. Simonneau, D. Bayart, *et al.*, "Impact of pump OSNR on noise figure for fiber-optical parametric amplifiers," IEEE Photonics Technol. Lett. **17**, 1178–1180 (2005).
29. R.-J. Essiambre, C. Guo, S. Kanth Dacha, *et al.*, "Record photon information efficiency with optical clock transmission and recovery of 12.5 bits/photon over an optical channel with 77 dB Loss," arXiv (2023).
30. M. Jarzyna, L. Kunz, W. Zwoliński, *et al.*, "Photon information efficiency limits in deep-space optical communications," Opt. Eng. **63**, 041209 (2024).
31. Z. Ye, P. Zhao, K. Twayana, *et al.*, "Overcoming the quantum limit of optical amplification in monolithic waveguides," Sci. Adv. **7**, eabi8150 (2021).
32. M. A. Butt, G. S. Voronkov, E. P. Grakhova, *et al.*, "Environmental monitoring: a comprehensive review on optical waveguide and fiber-based sensors," Biosensors **12**, 1038 (2022).
33. R. Larsson, R. U. Weerasuriya, and P. A. Andrekson, "Data - Ultralow noise preamplified optical receiver using conventional single wavelength transmission," Zenodo, 2024, https://doi.org/10.5281/zenodo.13872700.